Theoretical Modeling of Ethylene Insertion by Nickel Iminophosphonamide and Amidinate Complexes

Scott Collins*,† and Tom Ziegler*,‡

Department of Polymer Science, The University of Akron, Akron, Ohio 44325-3909, and Department of Chemistry, The University of Calgary, Calgary, Alberta T2N 1N4, Canada

Received August 15, 2007

Modeling of ethylene polymerization using density functional theory was undertaken for both generic and substituted nickel iminophosphonamide (PN_2) and amidinate (CN_2) complexes. The more highly substituted complexes were studied using quantum mechanics/molecular mechanics (QM/MM) techniques so as to probe the role of steric effects on insertion and chain-transfer processes. For the generic systems $H_2P(NSiH_3)_2NiR(L)$ and $HC(NSiH_3)_2NiR(L)$ (R = alkyl; L = C_2H_4), insertion had a higher barrier in the PN_2 versus CN_2 complex. The energy of ethylene binding was strongly affected by the nature of the R group. This was shown to be a function of agostic stabilization of the alkyl group in the absence of monomer. Insertion barriers are also strongly dependent on the nature of the alkyl group, particularly in the case of the sterically hindered Keim catalyst, which was modeled by $(Me_3Si)_2NP(Me)(NSiMe_3)_2NiR(L)$ and QM/MM techniques. Degenerate chain transfer was systematically studied in the case of the generic CN_2 complex $HC(NSiH_3)_2NiEt(C_2H_4)$ and proceeds through five-coordinate intermediates with distorted trigonal-bipyramidal geometries. The highest-energy intermediate corresponds to a bis(ethylene)−NiH complex, where loss of ethylene would constitute (degenerate) chain transfer. Intermediates in the analogous PN_2 complexes lie higher in energy, and thus these complexes should provide higher molecular weight material, as observed experimentally. β-H elimination/chain walking was also investigated using both generic and substituted complexes. The ground states in these reactions are agostic alkyls, while the ethylene−NiH complex, in which ethylene is perpendicular to the square plane, is a weakly bound intermediate. These intermediates are related to those formed during chain transfer by binding of the monomer.

1. Introduction

There is considerable interest in the synthesis of branched poly(ethylene) (PE) using transition-metal catalysts.[1] High-density and linear low-density PE, both with sparse long-chain branching, typically <1 long-chain branch (LCB) per 1000 C atoms, are produced using *ansa*-metallocene and constrained geometry catalysts in solution, slurry, or even gas-phase processes.[2] The mechanism of LCB formation in these materials primarily involves macromonomer incorporation,[3] a process that is facilitated by the "open" coordination sphere about the metal in these kinds of catalysts.

On the other hand, using α-diimine and related catalysts of Ni and Pd, branched PE is formed from ethylene by a chain-walking versus insertion mechanism.[4] Depending on the ratio of the rates of these two competing processes, materials that have controllable levels of short-chain branching (e.g., 0–100 Me groups per 1000 C atoms), depending on ethylene pressure, or materials with hyperbranched architecture[5] are available when the catalyst is capable of "walking" past a branch point at a rate that is much faster than that of insertion.

Stochastic simulations of chain growth using either kinetic[6] or density functional theory (DFT)[7] modeling approaches have failed to indicate the formation of LCBs (i.e., those with dimensions similar to those of the main chain) by a chain-walking versus insertion mechanism unless chain walking in a particular direction is favored. In essence, once a catalyst has migrated a few C atoms down the chain (or past a branch point), it becomes equally probable for it to walk in either direction. Thus, the chain-walking process becomes a true random walk, and it is expected that the formation of a long branch via such a process is improbable.

It is therefore of interest to note that the *first* synthesis of branched PE from ethylene monomer using a transition-metal catalyst, reported by Keim and co-workers nearly 25 years ago, was said to provide a material resembling *low-density* PE in its properties.[8] The catalyst was derived from the reaction of phosphorane **1** with either $Ni(COD)_2$ or $Ni(\eta^3\text{-}C_3H_6)_2$ in the presence of ethylene (eq 1).

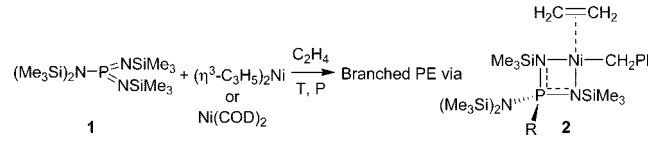

(1)

Subsequent work from the group of Yano in Japan has revealed that these catalyst formulations produce PE with methyl branches longer than six C atoms (Hx^+) as revealed by ^{13}C NMR analysis. Further, some of these branches were sufficiently long so as to influence the intrinsic viscosity in solution ($g' =$

* To whom correspondence should be addressed. E-mail: collins@uakron.edu (S.C.), ziegler@ucalgary.ca (T.Z.).
† The University of Akron.
‡ The University of Calgary.

10.1021/om700833b CCC: $37.00
Publication on Web 11/27/2007

$[\eta]_{br}/[\eta]_{lin} = 0.6–0.8$).[9] The group of Fink has shown that these formulations are competent for the chain-straightening oligomerization of α-olefins at low T and has postulated that this occurs via a chain-walking mechanism.[10]

As we recently reported, the active catalyst involved in these polymerization processes is an alkylnickel iminophosphonamide (PN_2) complex, $PN_2Ni(L)R$ (**2**; L = $H_2C{=}CH_2$) formed in situ from the phosphorane and either the Ni(0) or Ni(II) precursor (eq 1).[11] This was verified by the independent synthesis of two such complexes [$Ph_2P(NTMS)_2NiPh(PPh_3)$ (**2a**) and $Me(TMS_2N)P(NTMS)_2NiPh(PPh_3)$ (**2b**)]. These complexes form branched polymers with microstructures similar to, or in the case of **2b**, nearly identical with that produced using the Keim formulations. We have also shown that the PE produced using the Keim catalyst does possess sparse long-chain branching (by gel permeation chromatography light scattering) with properties resembling those of low-density PE;[11a,b] our modeling of polymer branching using a DFT-based stochastic simulation approach could not account for the intensity of Hx^+ branches in these materials as arising from a chain-walking versus insertion process, even though the short-chain branching distribution was reliably modeled. [The energetics of insertion versus chain walking for the Keim catalyst have been investigated in significant detail in connection with modeling of the branching distribution in PE formed using this catalyst.[11a] These calculations involved insertion of C_2H_4 into Ni−^{n}R, Ni−^{s}R, and Ni−^{t}R (R = Bu, amyl) and chain walking involving Ni−^{n}R, Ni−^{s}R, and Ni−^{t}R (R = Bu, amyl, hexyl). Details of these calculations are available from the authors upon request.]

Eisen and co-workers have reported polymerization studies using isoelectronic amidinate (CN_2) complexes of Ni [e.g., $PhC(NSiMe_3)_2Ni(acac)$], activated by methylaluminoxane

(1) (a) Stadler, F. J.; Piel, C.; Klimke, K.; Kaschta, J.; Parkinson, M.; Wilhelm, M.; Kaminsky, W.; Muenstedt, H. *Macromolecules* **2006**, *39*, 1474–1482. (b) Arikan, B.; Kaminsky, W. *Des. Monomers Polym.* **2005**, *8*, 589–600. (c) Zou, H.; Zhu, F. M.; Wu, Q.; Ai, J. Y.; Lin, S. A. *J. Polym. Sci., Part A: Polym. Chem.* **2005**, *43*, 1325–1330. (d) Li, H.; Stern, C. L.; Marks, T. J. *Macromolecules* **2005**, *38*, 9015–9027. (e) Bianchini, C.; Frediani, M.; Giambastiani, G.; Kaminsky, W.; Meli, A.; Passaglia, E. *Macromol. Rapid Commun.* **2005**, *26*, 1218–1223. (f) Wang, J.; Li, H.; Guo, N.; Li, L.; Stern, C. L.; Marks, T. J. *Organometallics* **2004**, *23*, 5112–5114. (g) Sworen, J. C.; Smith, J. A.; Berg, J. M.; Wagener, K. B. *J. Am. Chem. Soc.* **2004**, *126*, 11238–11246. (h) Capacchione, C.; Proto, A.; Okuda, J. *J. Polym. Sci., Part A: Polym. Chem.* **2004**, *42*, 2815–2822. (i) Sperber, O.; Kaminsky, W. *Macromolecules* **2003**, *36*, 9014–9019. (j) Heinicke, J.; Koehler, M.; Peulecke, N.; He, M.; Kindermann, M. K.; Keim, W.; Fink, G. *Chem.—Eur. J.* **2003**, *9*, 6093–6107. (k) Kasi, R. M.; Coughlin, E. B. *Macromolecules* **2003**, *36*, 6300–6304. (l) Kunrath, F. A.; Mota, F. F.; Casagrande, O. L.; Mauler, R. S.; de Souza, R. F. *Macromol. Chem. Phys.* **2002**, *203*, 2407–2411. (m) Komon, Z. J. A.; Diamond, G. M.; Leclerc, M. K.; Murphy, V.; Okazaki, M.; Bazan, G. C. *J. Am. Chem. Soc.* **2002**, *124*, 15280–15285. (n) Li, L.; Metz, M. V.; Li, H.; Chen, M.-C.; Marks, T. J.; Liable-Sands, L.; Rheingold, A. L. *J. Am. Chem. Soc.* **2002**, *124*, 12725–12741. (o) Schroeder, D. L.; Keim, W.; Zuideveld, M. A.; Mecking, S. *Macromolecules* **2002**, *35*, 6071–6073. (p) Galland, G. B.; Quijada, R.; Rojas, R.; Bazan, G.; Komon, Z. J. A. *Macromolecules* **2002**, *35*, 339–345. (q) Guan, Z. *Chem.—Eur. J.* **2002**, *8*, 3086–3092. (r) Coates, G. W.; Hustad, P. D.; Reinartz, S. *Angew. Chem., Int. Ed.* **2002**, *41*, 2236–2257. (s) Beigzadeh, D.; Soares, J. B. P.; Duever, T. A. *Macromol. Symp.* **2001**, *173*, 179–194. (t) Komon, Z. J. A.; Bazan, G. C. *Macromol. Rapid Commun.* **2001**, *22*, 467–478. (u) Gottfried, A. C.; Brookhart, M. *Macromolecules* **2001**, *34*, 1140–1142. (v) Walter, P.; Trinkle, S.; Suhm, J.; Mader, D.; Friedrich, C.; Mulhaupt, R. *Macromol. Chem. Phys.* **2000**, *201*, 604–612. (w) Hadjichristidis, N.; Xenidou, M.; Iatrou, H.; Pitsikalis, M.; Poulos, Y.; Avgeropoulos, A.; Sioula, S.; Paraskeva, S.; Velis, G.; Lohse, D. J.; Schulz, D. N.; Fetters, L. J.; Wright, P. J.; Mendelson, R. A.; Garcia-Franco, C. A.; Sun, T.; Ruff, C. J. *Macromolecules* **2000**, *33*, 2424–2436. (x) Held, A.; Mecking, S. *Chem.—Eur. J.* **2000**, *6*, 4623–4629. (y) Simon, L. C.; Mauler, R. S.; De Souza, R. F. *J. Polym. Sci., Part A: Polym. Chem.* **1999**, *37*, 4656–4663. (z) Mecking, S. *Macromol. Rapid Commun.* **1999**, *20*, 139–143.

(2) (a) Malmberg, A.; Kokko, E.; Lehmus, P.; Loefgren, B.; Seppaelae, J. V. *Macromolecules* **1998**, *31*, 8448–8454. (b) Harrison, D.; Coulter, I. M.; Wang, S.; Nistala, S.; Kuntz, B. A.; Pigeon, M.; Tian, J.; Collins, S. *J. Mol. Catal. A: Chem.* **1998**, *128*, 65–77. (c) Lai, S.-Y.; Wilson, J. R.; Knight, G. W.; Stevens, J. C.; Chum, P.-W. S. *PCT Int. Appl.* WO 9607680, 1996; 72. (d) Stevens, J. C. *Stud. Surf. Sci. Catal.* **1994**, *89*, 277–284. (e) Lai, S.-Y.; Wilson, J. R.; Knight, G. W.; Stevens, J. C. *U.S. Patent* 5,278,272, 1994; 14. (f) Lai,S.-Y.; Wilson, J. R.; Knight, G. W.; Stevens, J. C. *PCT Int. Appl.* WO 9308221, 1993; 82. (g) Stevens, J. C.; Timmers, F. J.; Wilson, D. R.; Schmidt, G. F.; Nickias, P. N.; Rosen, R. K.; Knight, G. W.; Lai, S.-Y. *Eur. Pat. Appl.* EP 416815, 1991; 58.

(3) (a) Simon, L. C.; Soares, J. B. P. *Ind. Eng. Chem, Res.* **2005**, *44*, 2461–2468. (b) Soares, J. B. P. *Macromol. Mater. Eng.* **2004**, *289*, 70–87. (c) Arjunan, P.; Dekmezian, A. H.; Markel, E. J.; Weng, W.; Garcia-Franco, C.; Jiang, P.; Soares, J. B. P.; Bonchev, D. *PMSE Prepr.* **2004**, *91*, 47–48. (d) Nele, M.; Soares, J. B. P. *Macromol. Theory Simul.* **2002**, *11*, 939–943. (e) Simon, L. C.; Soares, J. B. P. *Macromol. Theory Simul.* **2002**, *11*, 222–232. (f) Soares, J. B. P. *Macromol. Theory Simul.* **2002**, *11*, 184–198. (g) Soares, J. B. P. *Chem. Eng. Sci.* **2001**, *56*, 4131–4153. (h) Soares, J. B. P.; Penlidis, A. *Metallocene-Based Polyolefins* **2000**, *2*, 237–267. (i) Beigzadeh, D.; Soares, J. B. P.; Duever, T. A.; Hamielec, A. E. *Polym. React. Eng.* **1999**, *7*, 195–205. (j) Beigzadeh, D.; Soares, J. B. P.; Hamielec, A. E. *J. Appl. Polym. Sci.* **1999**, *71*, 1753–1770. (k) Beigzadeh, D.; Soares, J. B. P.; Hamielec, A. E. *Polym. React. Eng.* **1997**, *5*, 141–180.

(4) (a) Liu, W.; Brookhart, M. *Organometallics* **2004**, *23*, 6099–6107. (b) Leatherman, M. D.; Svejda, S. A.; Johnson, L. K.; Brookhart, M. *J. Am. Chem. Soc.* **2003**, *125*, 3068–3081. (c) Gottfried, A. C.; Brookhart, M. *Macromolecules* **2003**, *36*, 3085–3100. (d) Shultz, L. H.; Tempel, D. J.; Brookhart, M. *J. Am. Chem. Soc.* **2001**, *123*, 11539–11555. (e) Shultz, L. H.; Brookhart, M. *Organometallics* **2001**, *20*, 3975–3982. (f) Gottfried, A. C.; Brookhart, M. *Macromolecules* **2001**, *34*, 1140–1143. (g) Tempel, D. J.; Johnson, L. K.; Huff, R. L.; White, P. S.; Brookhart, M. *J. Am. Chem. Soc.* **2000**, *122*, 6686–6700. (h) Gates, D. P.; Svejda, S. A.; Onate, E.; Killian, C. M.; Johnson, L. K.; White, P. S.; Brookhart, M. *Macromolecules* **2000**, *33*, 2320–2334. (i) Svejda, S. A.; Johnson, L. K.; Brookhart, M. *J. Am. Chem. Soc.* **1999**, *121*, 10634–10635. (j) Tanner, M. J.; Brookhart, M.; DeSimone, J. M. *J. Am. Chem. Soc.* **1995**, *119*, 7617–7618. (k) Killian, C. M.; Tempel, D. J.; Johnson, L. K.; Brookhart, M. *J. Am. Chem. Soc.* **1996**, *118*, 11664–11665. (l) Johnson, L. K.; Killian, C. M.; Brookhart, M. *J. Am. Chem. Soc.* **1995**, *117*, 6414–6415.

(5) (a) Plentz-Meneghetti, S.; Kress, J.; Peruch, F.; Lapp, A.; Duval, M.; Muller, R.; Lutz, P. J. *Polymer* **2005**, *46*, 8913–8925. (b) Patil, R.; Colby, R. H.; Read, D. J.; Chen, G.; Guan, Z. *Macromolecules* **2005**, *38*, 10571–10579. (c) Guan, Z. *J. Polym. Sci., Part A: Polym. Chem.* **2003**, *41*, 3680–3692. (d) Guan, Z.; Cotts, P. M. *Polym. Mater. Sci. Eng.* **2001**, *84*, 382–383. (e) Cotts, P. M.; Guan, Z.; McCord, E.; McLain, S. *Macromolecules* **2000**, *33*, 6945–6952. (f) Guan, Z.; Cotts, P. M.; McCord, E. F.; McLain, S. J. *Science* **1999**, *283*, 2059–2062.

(6) (a) Soares, J. B. P.; Simon, L. C.; De Souza, R. F. *Polym. React. Eng.* **2001**, *9*, 199–223. (b) Simon, L. C.; Williams, C. P.; Soares, J. B. P.; de Souza, R. F. *Chem. Eng. Sci.* **2001**, *56*, 4181–4190. (c) Soares, J. B. P.; Simon, L. C.; De Souza, R. F. *AIChE J.* **2000**, *46*, 1234–1240.

(7) (a) Michalak, A.; Ziegler, T. *Organometallics* **2003**, *22*, 2069–2079. (b) Michalak, A.; Ziegler, T. *Macromolecules* **2003**, *36*, 928–933. (c) Michalak, A.; Ziegler, T. *J. Am. Chem. Soc.* **2002**, *124*, 7519–7528. (d) Michalak, A.; Ziegler, T. *J. Am. Chem. Soc.* **2001**, *123*, 12266–12278. (e) Michalak, A.; Ziegler, T. *Organometallics* **2000**, *19*, 1850–1858. (f) Woo, T. K.; Bloechl, P. E.; Ziegler, T. *J. Phys. Chem. A* **2000**, *104*, 121–129. (g) Michalak, A.; Ziegler, T. *Organometallics* **1999**, *18*, 3998–4004. (h) Deng, L.; Woo, T. K.; Cavallo, L.; Margl, P. M.; Ziegler, T. *J. Am. Chem. Soc.* **1995**, *119*, 6177–6186. (i) Deng, L.; Margl, P.; Ziegler, T. *J. Am. Chem. Soc.* **1995**, *119*, 1094–1100.

(8) Keim, W.; Appel, R.; Storeck, A.; Kruger, C.; Goddard, R. *Angew. Chem., Int. Ed. Engl.* **1981**, *20*, 116–117.

(9) (a) Yano, A.; Hasegawa, S.; Yamada, S. *Kobunshi Ronbunshu* **2002**, *59*, 377–381;cf. *Chem Abstr.* **137**, 201636. (b) Yano, A.; Yamada, S.; Yamada, K. *U.S. Patent* 5,324,799, 1994; 7 pp,Cont.-in-part of U.S. Series No. 662,167, abandoned. (c) Yano, A.; Yamada, S.; Yamada, K. *Eur. Pat. Appl.* 0446013, 1991; 8. (d) Yano, A.; Naito, Y.; Yamada, K.; Ohtsuru, M. *Eur. Pat. Appl.* 0381495, 1990; 7.

(10) (a) Möhring, V. M.; Fink, G. *Angew. Chem.* **1985**, *97*, 982–984. (b) Fink, G.; Möhring, V. M. *Patent Application* EP 01/94456 A2, 1986. (c) Schubbe, R.; Angermund, K.; Fink, G.; Goddard, R. *Macromol. Chem. Phys.* **1995**, *196*, 467–478.

(11) (a) Stapleton, R. A.; Chai, J.; Nuanthanom, A.; Flisak, Z.; Nele, M.; Ziegler, T.; Rinaldi, P. L.; Soares, J. B. P.; Collins, S. *Macromolecules* **2007**, *40*, 2993–3004. (b) Chai, J.; Flisak, Z.; Nele de Sousa, M.; Ziegler, T.; Soares, J. B.; Collins, S. *Polym. Prepr. (Am. Chem. Soc., Div. Polym. Chem.)* **2007**, *48*, 183–184. (c) Stapleton, R. A.; Chai, J.; Taylor, N. J.; Collins, S. *Organometallics* **2006**, *25*, 2514–2524. (d) Stapleton, R. A.; Nuamthanom, A.; Rinaldi, P. L.; Taylor, N. J.; Collins, S. *Polym. Prepr. (Am. Chem. Soc., Div. Polym. Chem.)* **2004**, *45*, 93–94.

(MAO).[12] These complexes provide *linear* unsaturated oligomers from ethylene at high activity in contrast to the branched polymer that is formed using the less active Keim catalyst. On the other hand, when unhindered Ni−PN_2 complexes are activated by MAO under the same conditions, they also provide oligomers (chiefly butenes) at high activity.[11c]

With a view to clarifying the intrinsic behavior of both Ni−CN_2 and Ni−PN_2 catalysts in ethylene polymerization, we elected to study both generic and substituted versions of these complexes by DFT using the quantum mechanics/molecular mechanics (QM/MM) hybrid approach for the latter systems. This paper reports on the structures and energies of these active species and the barriers to insertion, chain transfer, and chain walking.

2. Computational Details

All of the DFT results were obtained from calculations based on the Becke−Perdew exchange-correlation functional,[13] using the Amsterdam Density Functional (ADF) program.[14] The standard double-ζ Slater-type orbital (STO) basis sets with one set of polarization functions were applied for H, C, N, P, and Si atoms, while the standard triple-ζ basis sets were employed for the Ni atom.[15] The 1s electrons of C, N, and O as well as the 1s2p electrons of P, Si, and Ni were treated as frozen cores. Auxiliary s, p, d, f, and g STO functions,[16] centered on all nuclei, were used to fit the electron density and obtain accurate Coulomb and exchange potentials in each self-consistent-field cycle.

QM/MM modeling of the substituted catalysts [PhC{N-($SiMe_3$)}$_2$]NiR(L), [Ph_2P{N($SiMe_3$)}$_2$]NiR(L), and [(Me_3Si)$_2$-NP(Me){N($SiMe_3$)}$_2$]NiR(L) used the algorithms implemented within ADF,[17] where the QM part of these complexes were the generic complexes [HC{N(SiH_3)}$_2$]NiR(L), [H_2P{N(SiH_3)}$_2$]-NiR(L), and [(H_3Si)$_2$NP(H){N(SiH_3)}$_2$]NiR(L). Both the R group on Ni and L = C_2H_4 were treated using the full QM method, regardless of the chain length for the R group. Hence, the MM part consisted of substitution of C−H, Si−H, and P−H link atoms with C−Ph, Si−CH_3, and P−Ph or P−CH_3 groups, as appropriate. An augmented Sybyl force field[18] was utilized to describe the MM potential, which included van der Waals and torsional parameters for Si and P from the universal force-field (UFF) potential.[19]

The geometry optimization on the entire system was carried out with coupling between QM and MM atoms. In the optimization of the MM part, the C−C, Si−C, and P−C distances were constrained to be 41.0, 28.0, and 26.5% longer than the optimized C−H, Si−H, and P−H distances in the generic complex. These constraints were also based on the Sybyl or UFF bond-length values.[18,19] Electrostatic interactions were not included in the MM potential.

All structures reported here were stationary points on the potential energy surface based on minimization of the energy and energy gradients with respect to the Cartesian coordinates. For transition-state structures (denoted by TS), these were located initially by linear transit calculations along an assumed reaction coordinate. The geometry corresponding to an energy maximum was then subjected to transition-state optimization typically using a small step size (rad = 0.02). The approximate Hessian had one imaginary frequency or, if real, was essentially of zero magnitude. In selected cases, particularly during the study of conformationally complex systems, these stationary points were subjected to a constrained geometry optimization with the reaction coordinate fixed at the value located through transition-state optimization. If a lower -energy structure was located, this was resubjected to transition-state optimization in an iterative manner until no further change in the energy was observed.

3. Results and Discussion

Previous Experimental Data. As reported in detail elsewhere, the Keim catalyst is most efficiently generated in situ from Ni(COD)$_2$ and phosphorane **1**, usually in the presence of an α-olefin. The catalyst is unstable at room temperature with a peak turn-over frequency (TOF) of 225 h^{-1} at 25 °C and 30 psig C_2H_4 with [Ni] = [**1**] = 4 mM and [1-Hx] = 0.94 M.[11] Further, the activity of this catalyst is not a strong function of ethylene pressure (*P*) over the range studied (*P* = 30–450 psig), indicating that the propagation is zero-order in *P* or that saturation kinetics pertain.[20] Finally, in the absence of chain-transfer agents (i.e., α-olefins), the molecular weight (MW) of the PE formed varies between M_n = 30K and 100K with PDI = 2 depending on conditions, being lower in MW at lower *P*.

On the basis of the work of Fink and co-workers[10c] as well as our own studies, we have concluded that the extent of actual catalyst formation under these conditions is minimal. For example, at 20-fold higher concentrations of both Ni(COD)$_2$ and **1** in the presence of excess 1-hexene, ^{1}P NMR spectra indicate that the concentration of a $NiPN_2$ complex never exceeds ca. 9 mol % of the total amount of **1** added (see the Supporting Information). From this information, one can estimate that the intrinsic activity of the Keim catalyst at the lower concentrations reported in ref 11 corresponds to a TOF ≤ 1.25 s^{-1} or an insertion barrier of >17 kcal mol^{-1} at 298 K.

The modest dependence of MW on *P* (i.e., slightly higher at much higher *P*) suggests that chain transfer to monomer (or to α-olefin if present[11a]) is the principle process that limits chain growth. From the observed MW, the barriers to chain transfer can be inferred to be 2–4 kcal mol^{-1} higher in energy compared to insertion.

Both of the model complexes we prepared featured coordinated PPh_3, and both are essentially inactive in the absence of a PPh_3 scavenger. In the case of **2a**, Rh(I) had to be used, while in the case of **2b** in which PPh_3 is more labile, Ni(COD)$_2$ proved effective. In either case though, the activity of these two complexes was about 2 orders of magnitude lower than that of the Keim catalyst; because PPh_3 is a potent inhibitor of the Keim

(12) (a) Nelkenbaum, E.; Kapon, M.; Eisen, M. S. *J. Organomet. Chem.* **2005**, *690*, 3154–3164. (b) Nelkenbaum, E.; Kapon, M.; Eisen, M. S. *Organometallics* **2005**, *24*, 2645–2659.

(13) (a) Becke, A. *Phys. Rev. A* **1988**, *38*, 3098. (b) Perdew, J. P. *Phys. Rev. B* **1986**, *34*, 7406. (c) Perdew, J. P. *Phys. Rev. B* **1986**, *33*, 8822.

(14) (a) TeVelde, G.; Bickelhaupt, F. M.; Baerends, E. J.; Fonseca Guerra, C.; Van Gisbergen, S. J. A.; Snijders, J. G.; Ziegler, T. *J. Comput. Chem.* **2001**, *22*, 931. (b) te Velde, G.; Baerends, E. J. *J. Comput. Phys.* **1992**, *99*, 84. (c) Boerrigter, P. M.; te Velde, G.; Baerends, E. J. *Int. J. Quantum Chem.* **1988**, *33*, 87. (d) Versluis, L.; Ziegler, T. *J. Chem. Phys.* **1988**, *88*, 322. (e) Baerends, E. J.; Ellis, D. E.; Ros, P. *Chem. Phys.* **1973**, *2*, 41.

(15) Fonesca Geurra, C.; Visser, O.; Snijders, J. G.; te Velde, G.; Baerends, E. J. In *Methods and Techniques in Computational Chemistry METACC-95* Clementi, E., Corongiu, G., Eds.; STEF: Cagliari, Italy, 1995.

(16) Snijders, J. G.; Baerends, E. J.; Vernoijs, P. *At. Nucl. Data Tables* **1982**, *26*, 483.

(17) Woo, T. K.; Cavallo, L.; Ziegler, T. *Theor. Chem. Acc.* **1998**, *100*, 307.

(18) Clark, M.; Cramer, R. D., III; van Opdenbosch, N. *J. Comput. Chem.* **1989**, *10*, 982.

(19) Rappé, A. K.; Casewit, C. J.; Colwell, K. S.; Goddard, W. A., III; Skiff, W. M. *J. Am. Chem. Soc.* **1992**, *114*, 10024.

(20) Jenkins, J. C.; Brookhart, M. *J. Am. Chem. Soc.* **2004**, *126*, 5827–5842.

Table 1. DFT and Relative Energies of Generic X(NSiH$_3$)$_2$NiR(L) Complexes (for Structures, See Chart 1)

structure	R	L	total E (au)	ΔE (kcal mol^{-1})	structure	total E (au)	ΔE (kcal mol^{-1})	structure	total E (au)	ΔE (kcal mol^{-1})
3a	α-a-Me	α-CH	−4.185313[a]	32.8	**3b**	−4.176547[a]	35.5	**3c**	−5.529996[a]	34.6
4a	Me	C_2H_4	−4.237552	0	**4b**	−4.233057	0	**4c**	−5.585104	0
5a	Me	C_2H_4[b]	−4.225806	7.4	**5b**[b]	−4.213472	12.3	**5c**[b]	−5.564690	12.8
TS **6a**[c]	Me		−4.207527	18.8	TS **6b**[c]	−4.199137	21.3	TS **6c**[c]	−5.548893	22.7
7a	γ-a-^{n}Pr	γ-CH	−4.229455	5.1	**7b**	−4.222010	6.9	**7c**	−5.574838	6.4
8a	β-a-^{n}Pr	β-CH	−4.243499	−3.7	**8b**	−4.237187	−2.6	**8c**	−5.589967	−3.0
8d	β-a-Et	β-CH	−4.801333[a]	19.0	**8e**	−4.795288[a]	20.0	**8f**	−6.148318[a]	16.1
4d	Et[d]	C_2H_4	−4.831600	0	**4f**[d]	−4.827106	0	**4g**[d]	−6.174031	0
4e	Et[e]	C_2H_4	−4.829799	1.1						
5d	Et	C_2H_4[b]	−4.819433	7.7						
TS **6d**[c]	Et[d]		−4.801025	19.2	TS **6f**[c]	−4.790896	22.7	TS **6g**[c]	−6.141776	20.4
TS **6e**[c]	Et[e]		−4.800944	19.2						

[a] Total energy includes that of an isolated C_2H_4 molecule (QM E = −1.154766 au). [b] In-plane π complex. [c] Insertion transition state. [d] φ-axial Me group; see text. [e] φ-equatorial Me group; see text.

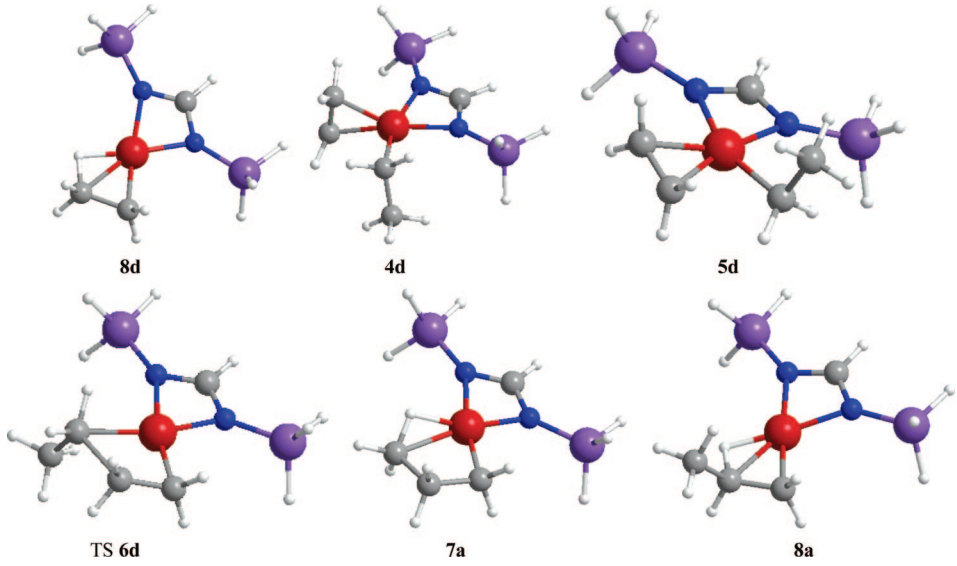

Figure 1. Representative structures of Ni−CN$_2$ complexes: β-agostic Ni−Et complex, **8d**; Ni−Et π complex (φ-axial Me group), **4d**; Ni−Et in-plane π complex (φ-axial Me group), **5d**; insertion TS (φ-axial Me group), TS **6a**; γ-agostic Ni−^{n}Pr complex, **7a**; β-agostic Ni−^{n}Pr complex, **8a**. For energies, see Table 1.

catalyst, we conclude that these low activities observed for the model complexes reflect *reversible* scavenging of PPh$_3$. Even so, the more sterically hindered complex **2b** formed PE that was 1–2 orders of magnitude higher in MW than that produced using **2a** and with a branching distribution strongly resembling that of the Keim formulations (i.e., both with ∼30 branches per 1000 C atoms with Me and Hx$^+$ branches in roughly equal amounts). The less hindered complex formed more highly branched PE (ca. 80 branches per 1000 C atoms) of lower MW ($\bar{X}_n \sim 20$).

In contrast, both this complex and other complexes featuring an unhindered PN$_2$ ligand can be activated for ethylene dimerization upon the addition of MAO (200 Al/Ni) at 25 °C and 150 psig. The peak activities are between 10^6 and 10^7 g of C_2H_4/mol of Ni × h, corresponding to a TOF of 10–100 s^{-1}. These data are comparable to that reported by Eisen and co-workers using benzamidinate complexes of Ni. Thus, the species responsible for ethylene oligomerization must have insertion barriers in the 15–16 kcal mol^{-1} range with relatively rapid rates of chain transfer.

DFT Modeling of Ethylene Insertion for Generic Complexes. Stationary points corresponding to agostic alkyls, π complexes, and insertion TS were located for the complexes X(NSiH$_3$)$_2$NiR(L) [R = Me, Et, ^{n}Pr; X = HC, H$_2$P, and H{(H$_3$Si)$_2$N}P; L = C_2H_4 or agostic C−H], and energies are depicted in Table 1, representative ball-and-stick structures are depicted in Figure 1, and a set of structures and the numbering scheme are shown in Chart 1.

Chart 1

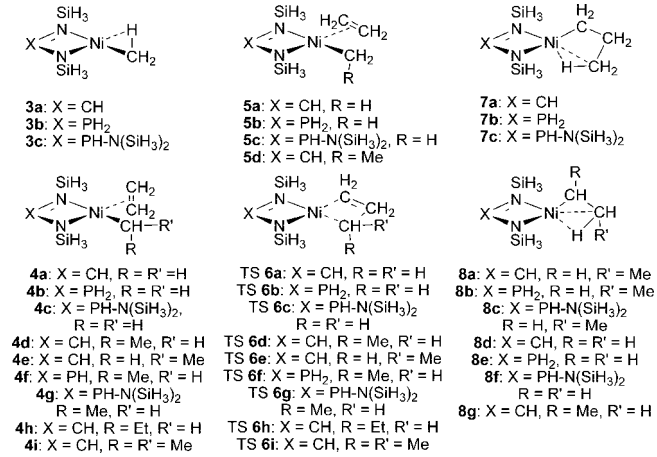

Binding of ethylene to the Ni−α-agostic Me (α-a-Me) complexes **3a**−**c** is strongly exothermic with a binding energy >30 kcal mol^{-1}. Ethylene binds most strongly when it is perpendicular to the square plane in π complexes **4a**−**c**; the corresponding in-plane π complexes **5a**−**c** were ca. 7 and 12–13 kcal mol^{-1} higher in energy for Ni−CN$_2$ versus Ni−PN$_2$

complexes. Surprisingly, the in-plane π complexes are local minima, as revealed by a frequency calculation on complex **5a**. We did not explore their conversion to **4** nor whether their formation was a prerequisite for ethylene insertion into Ni−Me (vide infra).

Insertion of ethylene into Ni−MeCN$_2$ complex **3a** involves a barrier of 18.8 kcal mol^{-1}. The transition-state geometry consists of a slightly puckered, four-membered ring. The Ni−C$_\alpha$ distances differ dramatically (1.896 vs 2.133 Å) in TS **6a** as do the C$_\alpha$−C$_\beta$ distances of 1.447 and 1.929 Å, where the longer distances involve the Me group undergoing migratory insertion. There is no evidence of an α-agostic interaction in the TS, as found for early metal systems, although the kinetic insertion product features a weak γ-agostic interaction (vide infra). Interestingly, the Ni−N distances of the CN$_2$ ligand are also distorted, with the Ni−N trans to the migrating group being much shorter than the other (1.918 vs 2.097 Å). The geometry of the transition structure TS **6a** resembles that located earlier for nickel diimine or anilinotroponate complexes;[7] it is also perhaps worth noting that the insertion barriers are not very different from those estimated by DFT methods for insertion involving nickel anilinotroponate complexes.

The immediate product following insertion into the Ni−Me bond are γ-a-^{n}Pr complexes **7a**−**c**, which lie 5–7 kcal mol^{-1} higher in energy than the corresponding π complexes; however, these can quickly relax to β-a-^{n}Pr structures **8a**−**c** by simple rotation about the C$_\beta$−C$_\gamma$ bond. These β-agostic complexes are between 2.5 and 4.0 kcal mol^{-1} lower in energy than the starting π complexes so that the overall propagation reaction is exothermic by at least 22 kcal mol^{-1}.

The geometrical features of the corresponding alkyls, π complexes, and insertion TS for the two PN$_2$ complexes investigated were analogous to those just discussed for the CN$_2$ complex. However, significant energetic differences are observed with 2.5–3.9 kcal mol^{-1} higher insertion barriers, relative to the π complexes **4b** and **4c**, and 1.8–2.7 kcal mol^{-1} more exothermic binding of ethylene to the Ni−Me complexes **3b** and **3c**.

We suspect that the higher insertion barriers, as well as the increased exothermicity, on binding of ethylene to PN$_2$ versus CN$_2$ complexes reflect the more electron-rich nature of the former ligands. It is known that the thermodynamic basicities of these two ligands differ by about 3 orders of magnitude;[21] presumably, coordination of ethylene stabilizes the resulting π complexes through back-donation because neither the CN$_2$ nor the PN$_2$ ligands are strong π acceptors. Because this stabilizing interaction is reduced or eliminated in the TS for insertion, the increased insertion barriers for PN$_2$ versus CN$_2$ complexes are expected. It should be noted that the in-plane π complexes for both PN$_2$ complexes **5b** and **5c** were 5 kcal mol^{-1} less stable with respect to the most stable π complexes, compared to the corresponding CN$_2$ structure **5a**, confirming the importance of back-bonding when ethylene is in a perpendicular orientation.

Binding of ethylene to Ni−β-a-Et complexes **8d**−**f** was also investigated and is significantly less exothermic with ΔE = 16–20 kcal mol^{-1}. We attribute this large difference in the binding energy to the enhanced stability of the higher alkyl complexes that can adopt β-agostic structures. We note that (at least) two diastereomers are possible for the π complexes **4** in the case of the Ni−Et complexes **8d**−**f**. They differ in the orientation of the Me of the Et group being in-plane (or φ-equatorial in **4e**) versus out-of-plane (or φ-axial in **4d**, **4f**, and **4g**). In the case of the π complexes **4e** and **4d**, the latter is more stable (by 1.1 kcal mol^{-1}).

Insertion of ethylene into Ni−Et complex **8d** involves a barrier of 19.2 kcal mol^{-1}, and as with the π complexes, there are two stereoisomeric transition structures TS **6d** and TS **6e** differing in the orientation of the Me group. The energies of these structures are essentially equivalent in this case. While this observation is not that important here, it has major consequences when looking at the more highly substituted systems, as will be explained later.

Steric effects manifest themselves in two ways in the case of the more highly substituted complex **8f**. Binding of ethylene is significantly less exothermic (by 3–4 kcal mol^{-1}) compared to that of complexes **8d** and **8e**. We attribute this to destabilization of the π complex **4g** because the coordinated ethylene and the φ-axial Me group experience interactions with both the in-plane and out-of-plane SiH$_3$ moieties.

It should be noted that the presence of the N(SiH$_3$)$_2$ substituent on P has an effect on the location of the in-plane NSiH$_3$ groups in that the PN$_2$Ni ring is slightly puckered (dihedral angle φ = 171.6°) compared to essentially planar in the less substituted systems. In essence, the in-plane SiH$_3$ groups tilt away from the N(SiH$_3$)$_2$ moiety, and thus there is hindrance both above and below the square plane in **8f**.

Similarly, insertion into Ni−Et in the case of **8f** features a 2.3 kcal mol^{-1} lower barrier than insertion involving **8e**, while the difference in insertion barriers between **8d** and **8e** (ΔE = 3.5 kcal mol^{-1}) was comparable to that observed for **3a** and **3b** (2.5 kcal mol^{-1}). Because steric hindrance above and below the square plane is partially relieved in the transition state for insertion, the barrier is correspondingly reduced in the case of TS **6g**. Even though the Me group of the Et moiety is φ-axial in both the most stable π complex and insertion TS, the Et group is much further away from Ni in the TS and so steric interactions with the larger PN$_2$ ligand are largely alleviated.

DFT Modeling of Chain Transfer in Generic Complexes. Chain transfer to monomer in nickel diimine catalysts has been investigated previously and proceeds through bis(olefin) hydride complexes.[7] We investigated the analogous process here but in the context of degenerate transfer starting from the CN$_2$−NiEt π complex. This process initiates by establishing an agostic interaction between the Ni−Et group above or below the square plane of the π complex. While this motion should lead to a square-pyramidal (spy) intermediate, attempts to locate such stationary points were unsuccessful; optimizations refined to either the π complex **4d** or a distorted trigonal-bipyramidal (tbp) complex **9a** that lies 4.2 kcal mol^{-1} higher in energy. This complex features an apical Ni−CH$_2$CH$_3$ group with an equatorial Ni−β-a-CH interaction (Figure 2 and Chart 2).

A much higher energy tbp intermediate **10a** is isomeric and features an equatorial Ni−CH$_2$CH$_3$ with an apical Ni−β-a-CH interaction; it is 14.9 kcal mol^{-1} higher in energy than the most stable π complex **4d**. Another intermediate **11a** that can be formed from **10a** by β-H elimination is of nearly identical energy (ΔE = 15.0 kcal mol^{-1} with respect to **4d**) and is best described as a tbp bis(ethylene)−NiH complex featuring two equatorial ethylene molecules and an apical Ni−H. Both of the ethylene molecules are orthogonal to Ni−H and are essentially equivalent by symmetry.

A final stationary point **12a** was located in which one of the ethylene molecules has rotated so that it is coplanar with Ni−H. This structure lies 4.7 kcal mol^{-1} higher in energy than **11a**, and a frequency calculation indicated that it is a local minimum.

(21) (a) Review: Kabachnik, M. I. *Phosphorus Relat. Group V Elem.* **1971**, *1*, 117–132. (b) Genkina, G. K.; Korolev, B. A.; Gilyarov, V. A.; Stepanov, B. I.; Kabachnik, M. *Z. Obsh. Khim.* **1969**, *39*, 326–329.

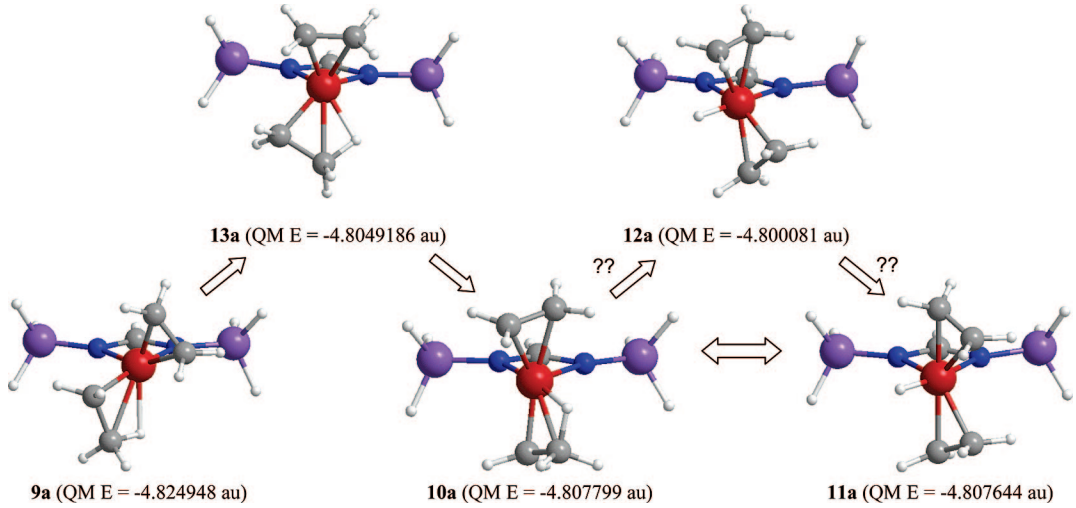

Figure 2. Intermediates **9a**−**13a** involved in degenerate chain transfer to monomer for the $CN_2NiEt(C_2H_4)$ complex. See the text for an explanation of the individual structures.

Chart 2

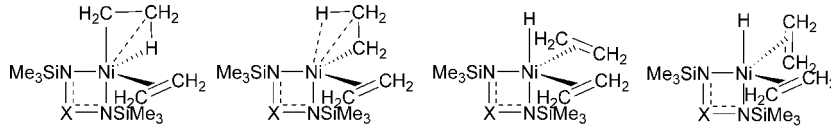

Scheme 1. Chain Transfer in Ni−CN_2 and PN_2 Complexes

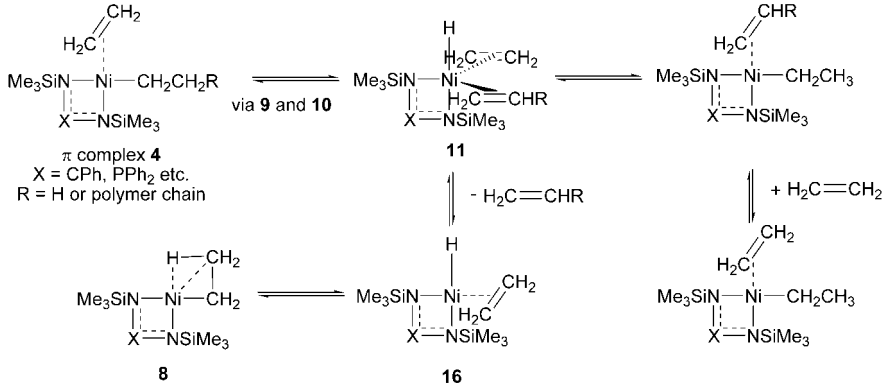

It is unclear whether this intermediate is involved in chain transfer. It is also possible to transform **11a** directly into **10a** merely by rotating one of the coordinated ethylene molecules about the metal. This pathway was investigated by linear transit and has a barrier less than 4.7 kcal mol^{-1}; **12a** is not an intermediate structure involved in this pathway. We shall return to the nature of **12a** when we discuss chain transfer in the substituted complexes.

The pathway from intermediate **9a** to furnish **10a** proved problematic to locate. Although, in principle, these complexes may interconvert through φ-rotation, the requisite spy intermediates do not represent stationary points on the potential energy surface (or they are so weakly bound that they cannot be located using conventional algorithms based on steepest descent). A structure intermediate between **9a** and **10a** and involving rotation of the CN_2 ligand about the Ni---C axis was located by linear transit techniques. Transition-state optimization of this structure using a small step size converged to structure TS **13a** (QM $E = -4.804919$ au), which resembles a trigonal prism (Figure 2), and is only 1.8 kcal mol^{-1} higher in energy than intermediate **10a**. A frequency calculation on TS **13a** revealed one imaginary frequency consistent with this transition structure being intermediate between **9a** and **10a**.

All of the stationary points identified in connection with the formation of intermediate **11a** are local minima on the potential energy surface as revealed by frequency calculations except for TS **13a**. Undoubtedly, there are other transition structures connecting these shallow minima, but we were unsuccessful in locating them. For example, the highest-energy structure in a linear transit between **11a** and **10a** when subjected to unrestrained optimization converged to either of these high-energy intermediates.

To summarize, degenerate chain transfer proceeds via the establishment of an agostic interaction, above or below the square plane, and then isomerization to a high-energy tbp intermediate. A low barrier separates this latter species from a bis(olefin) hydride complex, where the two ethylene molecules are equivalent. Of course, in the real situation, one of these coordinated alkenes will be a polymer chain with terminal or even internal unsaturation. Reversal of these steps will lead to

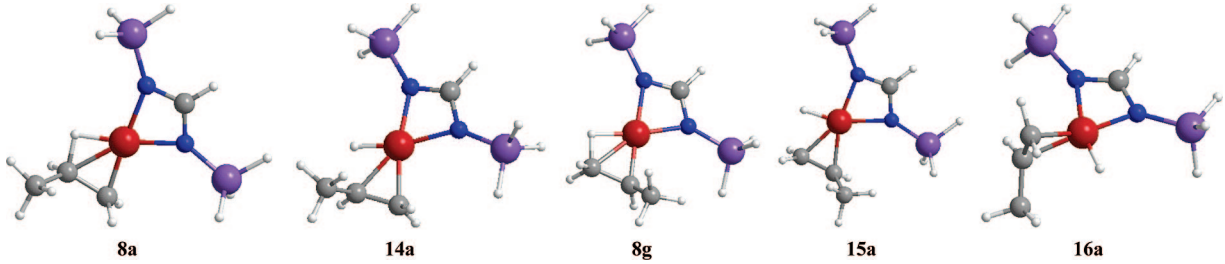

Figure 3. Agostic ^{n}PrNiCN$_2$ complex **8a**, in-plane π complex **14a**, agostic ^{i}Pr complex **8g**, in-plane π complex **15a**, and out-of-plane NiH(C$_3$H$_6$) π complex **16a** (*syn*-Me group). For energies, see Table 2.

Table 2. DFT and Relative Energies for HC(NSiH$_3$)$_2$NiR(L) Complexes

structure	R	L	total E (au)	ΔE (kcal mol^{-1})	total E + C$_2$H$_4$ (au)	ΔE (kcal mol^{-1})
8a	β-a-^{n}Pr	β-CH	−4.243552	0.22	−5.398318	18.3
8g	β-a-^{i}Pr	β-CH	−4.243908	0.00	−5.398674	18.1
14a[a]	H	C$_3$H$_6$	−4.235236	5.44	−5.390002	23.5
15a[b]	H	C$_3$H$_6$	−4.237012	4.33	−5.391778	22.4
syn-Me **16a**	H	C$_3$H$_6$	−4.236404	4.71	−5.391150	22.8
anti-Me **17a**	H	C$_3$H$_6$	−4.236206	4.83	−5.390968	22.9
4h	^{n}Pr	C$_2$H$_4$	−5.427482	0.00	−5.427482	0.00
4i	^{i}Pr	C$_2$H$_4$	−5.426859	0.39[c]	−5.426859	0.39
insertion TS **6h**	^{n}Pr		−5.397305	18.9[c]	−5.397305	18.9
insertion TS **6i**	^{i}Pr		−5.396323	19.6[c]	−5.396323	19.6

[a] In-plane π complex with two imaginary frequencies, the lowest of which involves C−H stretching of the agostic C−H. [b] In-plane π complex with no imaginary frequencies based on the approximate Hessian. [c] Relative energy with respect to the most stable π complex **4h**.

a Ni−Et π complex with the chain still coordinated (Scheme 1). Actual chain transfer will not occur unless the chain end is ejected from an intermediate analogous to **11a** (and a complex analogous to **12a** may be an intermediate involved in this pathway). Alternately, associative substitution of the coordinated chain end by ethylene is possible from the π complex, as suggested by Brookhart and co-workers.[4]

Structure **12a** represents the highest energy stationary point located in the case of Ni−CN$_2$ complexes in the context of chain transfer. It is 19.8 kcal mol^{-1} higher in energy than the most stable π complex, while insertion features a comparable barrier of 19.0 kcal mol^{-1}. Assuming that chain transfer to monomer is the only process occurring with the systems studied by Eisen and co-workers and that propagation is first-order in [Ni] but zero-order in [M], the number-average degree of polymerization will be

$$\bar{X}_n = \frac{R_p}{R_{tr}} = \frac{k_2[\mathrm{Ni{\bullet}C_2H_4}]}{k_{tr}[\mathrm{Ni{\bullet}C_2H_4}]} \approx \frac{k_2}{k_{tr}} \qquad (1)$$

where k_2 is the insertion and k_{tr} is the transfer rate constant. It is obvious that the generic complex would only oligomerize ethylene with $\bar{X}_n \sim 3.85$ at 298 K. This is fortuitously close to that observed in the real systems studied by Eisen and co-workers.

Chain transfer was also studied in the context of the other generic π complexes **4f** and **4g** under investigation. In the case of π complex **4f**, structure **12b** (QM $E = -4.786112$ au) is 25.7, while the corresponding insertion TS **6f** is 22.8 kcal mol^{-1} higher in energy. A similar difference in energy is seen for π complex **4g**, where insertion TS **6g** and structure **12c** (QM $E = -6.137162$ au) are 20.4 and 23.1 kcal mol^{-1} higher in energy, respectively. Thus, in both cases, insertion is favored over chain transfer by ~3 kcal mol^{-1}, which corresponds to $\bar{X}_n \sim 157$ at 298 K. Thus, both complexes should polymerize ethylene to a low-MW polymer ($\bar{M}_n \sim 4400$) at 298 K.

DFT Modeling of Chain Isomerization in Generic Ni−CN$_2$ Complexes. Chain isomerization involving reversible β-H elimination and reinsertion into Ni−H is the key process involved in chain walking.[4,7] It was investigated for Ni−Et, Ni−^{n}Pr, and Ni−^{i}PrCN$_2$ complexes, although only the latter two complexes (**8a** and **8g**) are discussed here. The ground-state structures involved in chain walking are agostic alkyls **8a** and **8g** (Figure 3), where β-H elimination proceeds via transient in-plane Ni−H(C$_3$H$_6$) complexes **14a** and **15a**. These complexes or the agostic alkyls can isomerize to out-of-plane π complexes **16a** and **17a** (Table 2, Figure 3, and Scheme 2) by rotation of coordinated olefin.

Unlike the situation encountered for nickel alkyls, it would appear that in-plane π complexes **14a** and **15a** are transition structures; a frequency calculation on **14a** indicated two imaginary frequencies, the lowest energy of which corresponds to stretching of the agostic C−H bond in **8a**. The next imaginary frequency involved SiH$_3$ rotation, was of low intensity, and is not relevant. However, the energy of **15a** (located via TS optimization) is actually somewhat *lower* than either of the out-of-plane π complexes **16a** and **17a**, while the approximate Hessian had no imaginary frequencies. A linear transit calculation starting from **8g**, and stretching of the agostic C−H bond revealed an inflection point at the geometry corresponding to **15a** but no minimum.

It is unclear whether **14a** and **15a** are relevant stationary points involved in chain walking. The agostic alkyls and out-of-plane π complexes can directly interconvert by rotation of coordinated alkene about the metal, and neither of these in-plane structures is encountered during this process. In the case of the generic NiCN$_2$ Pr complexes **8a** and **8g**, this was investigated by linear transit; the barriers to this rotation are between 5.1 and 5.4 kcal mol^{-1}, with π complex **16a** a high-energy intermediate (Figure 4).

Summarized in Table 2 are the absolute and relative energies for the Ni−^{n}Pr and ^{i}Pr complexes along with relevant data for ethylene binding and insertion. On a strictly enthalpic basis (last two columns of Table 2), chain walking features significantly higher barriers than insertion (by 3–4 kcal mol^{-1}) such that one would be tempted to predict that only linear oligomers would be formed from this generic Ni−CN$_2$ complex. However, this

Scheme 2. Chain-Walking Isomerization of $NiCN_2$ Propyl Complexes

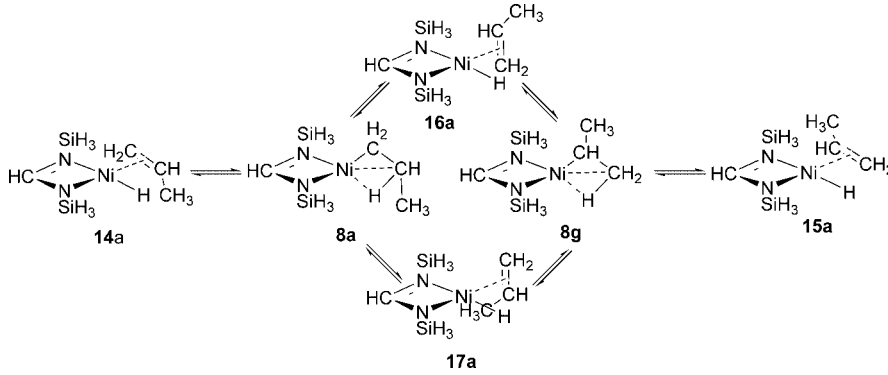

analysis neglects the significant entropy change on ethylene binding to the agostic alkyls. This value has been estimated both experimentally and theoretically to correspond to ~9.0 kcal mol^{-1} at 298 K.[4,7]

Under such a scenario, ejection of ethylene from the most stable π complexes will be the rate-determining step involved in chain walking with barriers of 18.3 and 18.1 kcal mol^{-1} for ^{n}Pr and ^{i}Pr, respectively (Scheme 3). In contrast, the out-of-plane π complexes involved in chain walking will be only 13.8–14.1 kcal mol^{-1} higher in energy than the most stable π complexes. Thus, a consideration of *free energy* changes in insertion versus chain walking would seem to indicate that the generic $Ni-CN_2$ complexes should be quite competent for the latter event.

Analogous calculations on the generic PN_2 complexes were not performed. Instead, attention was next focused on the study of the "real" catalysts through the introduction of substituents and the use of QM/MM techniques to model electronic and steric effects with these catalysts.

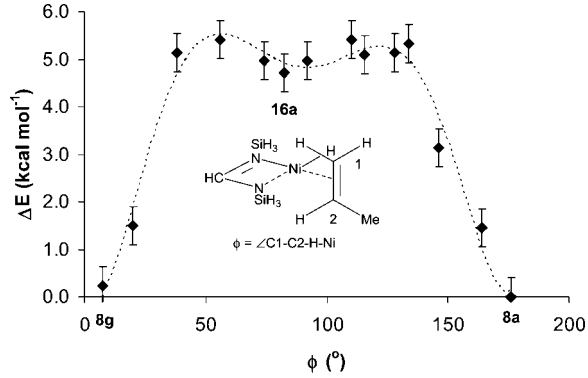

Figure 4. Linear transit between β-agostic $HCN(SiH_3)_2NiPr$ complexes **8a** and **8g** involving rotation of C_3H_6 about the Ni−H bond. π complex **16a** is an intermediate along this pathway. The dashed line is a fit of a sixth-order polynomial to the data points, where an approximate error of ±0.4 kcal mol^{-1} is implied.

Scheme 3. Chain-Walking versus Insertion Energetics for $HC(NSiH_3)_2NiPr$ Complexes

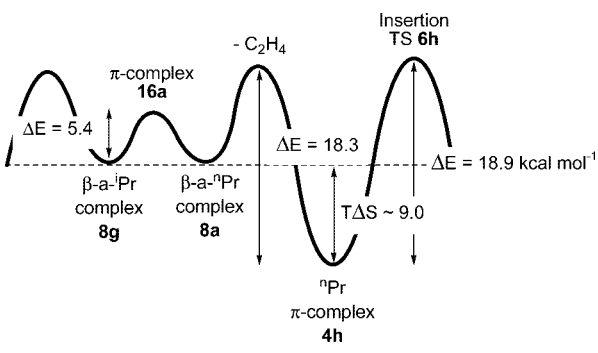

QM/MM Modeling of Insertion and Chain Transfer for $Ni-CN_2$ versus PN_2 Complexes. These two processes were studied for $X(NSiMe_3)_2NiEt$ complexes where X = CPh (**8a**−Ph), PPh_2 (**8b**−Ph_2), and $PMe[N(SiMe_3)_2]$ (**8c**−Me). Because the latter complex features unsymmetrical environments above and below the square plane, this doubles the number of configurations that need to be examined by QM/MM techniques. In most cases, location of the substituents, etc., on the least hindered side of the square plane, syn to the P−Me group, was considered when modeling insertion and chain transfer.

Shown in Figure 5 are the structures of the relevant intermediates involved in these processed for the $Ni-CN_2$ complex. The structures of the PN_2 complexes are analogous and the energies of all of these structures are summarized in Table 3 along with those of the generic complexes for comparison. Finally, we include Chart 3 showing the QM/MM structures involved in insertion and chain transfer along with a numbering scheme.

There are two major effects of replacing Si−H with $Si-CH_3$ groups in these molecules, as well as including the appropriate substituents on C or P. There is a reduction in the binding energy of ethylene to the agostic alkyls in the case of the hindered $Ni-CN_2$ and $Ni-PN_2$ complexes of ca. 1.5–2.5 kcal mol^{-1}. The exception to this trend is found for **8f**−Me, where binding of ethylene is about 1.5 kcal mol^{-1} more exothermic than that in the generic system. The other effect is a fairly dramatic change in the energies of the structures corresponding to **12**, thought to be involved in chain transfer, relative to the most stable π complex.

As for the reduction in ethylene binding energy, an examination of the energies of the agostic alkyls and their corresponding π complexes reveals no clear trends. In the case of the $Ni-CN_2$ complexes, the QM energies of the agostic alkyls in the generic **8d** and substituted systems **8d**−Ph are nearly equivalent (Table 3), and it is the π complex **4d**−Ph that is destabilized in the case of the real catalyst. However, the converse situation is true for the unhindered $Ni-PN_2$ complex **8e** and **8e**−Ph_2.

We do note that the different "bite" angles of these two ligands (~68 vs 78° for $Ni-CN_2$ vs $Ni-PN_2$ complexes) lead to differences in the in-plane steric effects. In essence, in the $Ni-CN_2$ complexes, the $N-SiMe_3$ groups are further away (by ca. 0.3 Å) from the remaining ligands than in the case for the $Ni-PN_2$ complex. This feature should selectively destabilize the agostic ethyl complex, where all of the atoms are in-plane, in the case of the $Ni-PN_2$ complex as observed.

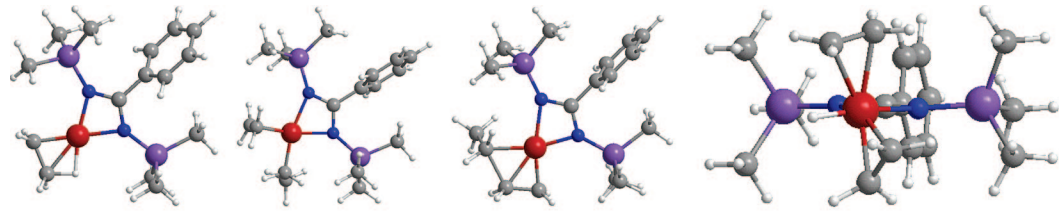

Figure 5. Structures of NiEt **8d**−Ph, NiEt(C_2H_4) **4d**−Ph, NiEt insertion TS **6d**−Ph, and NiEt chain-transfer intermediate **12a**−Ph for Ph-substituted Ni−CN_2 complexes.

Table 3. DFT Energies for Ni−CN_2 and Ni−PN_2 Complexes Modeled by QM/MM Techniques

generic structure	QM E (au)	ΔE (kcal mol^{-1})	real structure	QM E (au)	ΔE (kcal mol^{-1})
8d (+C_2H_4)	−4.801333	19.0	**8d**−Ph (+C_2H_4)	−4.801087	17.5
π complex **4d** (L = C_2H_4)	−4.831600	0.0	π complex **4d**−Ph	−4.828960	0.0
insertion TS **6d**	−4.801025	19.2	insertion TS **6d**−Ph	−4.797909	19.5
chain-transfer TS **12a**	−4.800081	19.8	chain-transfer TS **12a**-Ph	−4.798409	19.2
8e (+C_2H_4)	−4.795288	20.0	**8e**−Ph_2 (+C_2H_4)	−4.800446	17.5
π complex **4f**	−4.827106	0.0	π complex **4f**−Ph_2	−4.828404	0.0
insertion TS **6f**	−4.790896	22.7	insertion TS **6f**−Ph_2	−4.792125	22.8
chain-transfer TS **12b**	−4.786112	25.7	Chain transfer TS **12b**−Ph_2	−4.796860	19.8
8f (+C_2H_4)	−6.148318	16.1	**8f**−Me (+C_2H_4)	−6.156050	17.6
π complex **4g**	−6.174031	0.0	π complex **4g**−Me	−6.184073	0.0
insertion TS **6g**	−6.141776	20.2	insertion TS **6g**−Me	−6.153765	19.0
chain-transfer TS **12c**	−6.137162	23.1	chain-transfer TS **12c**−Me	−6.131615	32.9
			chain-transfer TS **12c**−Me′[a]	−6.143770	25.3

[a] Highest-energy structure on linear transit between structures **11c**−Me (QM E = −6.149458 au) and **10c**−Me (QM E = −6.151816 au; Chart 3) involving rotation of one coordinated ethylene about Ni−H in **11c**−Me.

Chart 3

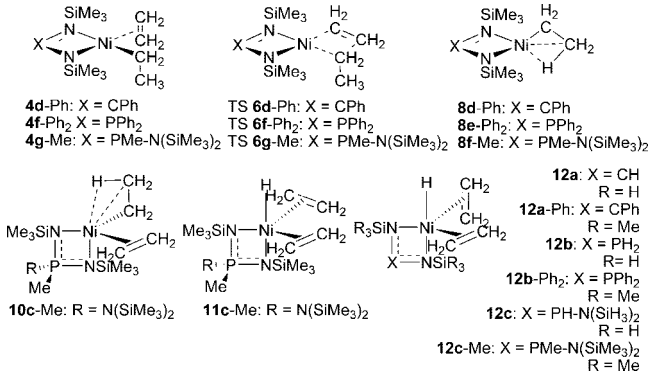

In the case of the hindered Keim catalyst, ethylene binding energies increase by 1.5 kcal mol^{-1} compared to a generic system featuring an $N(SiH_3)_2$ substituent on P. An examination of the energies indicates that both the π complex **4g**−Me and agostic ethyl **8f**−Me are stabilized by a similar amount in the hindered catalyst, although the difference is largest with the π complex (6.3 vs 4.8 kcal mol^{-1}). This result seems counterintuitive given the increased steric hindrance at least on one side of the square plane in the Keim catalyst.

Much more dramatic effects were noted on the energies of the structures corresponding to **12**, earlier identified as the highest-energy stationary point involved in chain transfer with the generic Ni−CN_2 complex. Surprisingly, there is a significant decrease in the energy (nearly 6 kcal mol^{-1}) of this transition structure in the case of the Ni−PN_2 complex **12b**−Ph_2 versus the generic system **12b**. An examination of these two structures reveals that, in the latter case, the weakly coordinated ethylene molecule is nearly coplanar with the Ni−H bond (φ = 0.62°), while in the case of the substituted system, it is slightly twisted (φ = 15.1°). Because the energies of the Ni−CN_2 complexes **12a** and **12a**−Ph are nearly equivalent and this dihedral angle also has a similar value for both (3.2 vs 5.8°), we conclude that the energy of this structure is a sensitive function of the twist angle because of repulsive interactions of the ethylene π electrons with the Ni−H σ bond. In fact, an optimization for Ni−PN_2 complex **12b**−Ph_2, where this dihedral was restrained at 0°, converged to a structure that was 22.2 kcal mol^{-1} higher in energy than the π complex **4f**−Ph_2.

On the other hand, in the case of the hindered Keim catalyst, the energy of structure **12c**−Me is nearly 10 kcal mol^{-1} higher compared with the energy of the generic system **12c**. Because the structures of these two stationary points were otherwise similar, we conclude that steric effects are responsible for the destabilization seen. Specifically, because the ethylene molecules are located above and below the plane defined by Ni, H, and the two N atoms, at least one of them will experience steric hindrance due to the bulky $N(SiMe_3)_2$ group.

In contrast, insertion barriers were largely unaffected in going from the generic to the substituted systems. There was a modest decline of 1.2 kcal mol^{-1} in the barrier for the hindered Keim catalyst. As mentioned previously, the π complex **4g**−Me is more stable than **4g** by ca. 6.3 kcal mol^{-1}, while the transition state for insertion TS **6g**−Me is lowered by an even larger amount (7.5 kcal mol^{-1}), thus accounting for the modest decline in insertion barriers.

It should be noted, however, that the geometry of the insertion TS in the case of TS **6g**−Me differs significantly from many of the other complexes studied. The four-membered $NiCH_2CH_2$(μ-Et) ring is more puckered with a dihedral angle of 159° vs 164° in the generic complex TS **6g**, such that the Et group undergoing migratory insertion lies significantly below the square plane [syn to the P−Me group and away from the bulky $N(SiMe_3)_2$ moiety].

The other transition structures featured dihedral angles between 163 and 180°, where the most acute angle was observed for $NiPN_2$ complex TS **6f**−Ph_2. Thus, substitution above and/or below the square plane causes this puckering, and this effect

may well be indirect in that these substituents, in turn, influence the conformation of the in-plane $NSiR_3$ groups bonded to the metal (vide supra).

Thus, the effects of ligand substitution are most profound in the case of the Keim catalyst, less so for the unhindered PN_2 complex, and least evident for the CN_2 complex. In absolute terms, the DFT QM/MM results suggest that the Keim catalyst **4g**−Me would be most active with, or at least of comparable activity to, the CN_2 system **4d**−Ph. The unhindered PN_2 catalyst **4f**−Ph_2 would be the least active and by a considerable margin (ca. 600 times less active at 298 K than **4g**−Me). The actual insertion barrier of 19.0 kcal mol^{-1} for the Keim catalyst agrees reasonably well with that estimated from the peak TOF and a catalyst concentration at 298 K (vide supra). On the other hand, there is a significant discrepancy between the calculated insertion barrier for the amidinate catalyst and what can be estimated from the work of Eisen and co-workers.

As far as the MW of the polymer is concerned, the DFT QM/MM results indicate that the Keim catalyst **4g**−Me should produce the highest-MW polymer by far, in agreement with the experimental results. In fact, if **12c**−Me was the actual TS for chain transfer, $\bar{X}_n$ would be in excess of 10^{10} at 298 K. Because the observed MW in the absence of α-olefin corresponds to $\bar{X}_n \sim 10^3$, this implies that the chain transfer and insertion barriers differ by only 4.6 kcal mol^{-1}.

One can also view **12c**−Me as an intermediate involved in ethylene binding to the high-energy olefin hydride complexes **16** and **17** involved in chain walking (vide supra). In this sense, the observed ordering in energy reflects what one would intuitively expect for associative substitution on such intermediates but may not be relevant for actual chain transfer. It is interesting to note that analogous structures could not be located for olefin−alkyl intermediates; we note that one of the coordinated ethylene molecules in **12c**−Me is weakly bound (Ni−C > 2.2 Å) and in the more hindered alkyl complexes may dissociate completely.

It is thus possible that chain transfer proceeds as previously described but does not involve **12** as an intermediate. Indeed, a linear transit calculation on the hindered Keim catalyst going from intermediate **11c**−Me to **10c**−Me, which are 21.7 and 20.2 kcal mol^{-1}, respectively, higher in energy relative to the most stable π complex **4g**−Me (see the footnote to Table 3) and which involved rotation of one coordinated ethylene into coplanarity with Ni−H, revealed a significantly lower internal barrier (3.6 kcal mol^{-1} with respect to **11c**−Me), where the highest-energy point (**12c**−Me′) was now 25.3 kcal mol^{-1} above the most stable π complex (Table 3).

Chain Walking for Substituted Ni−CN_2 versus PN_2 Complexes. This was studied by examining isomerization of agostic Ni−^{n}Bu to Ni−^{s}Bu complexes and degenerate isomerization of the latter. The motion was analogous to that studied in the generic systems and involved rotation of 1- or *trans*-2-butene about the Ni−H axis. We did not consider the process involving *cis*-2-butene, but it obviously can occur.

As shown in Scheme 4, even for the two symmetrical catalysts, there are two ways in which one can go from Ni−^{n}Bu complex **8h** to Ni−^{s}Bu complex **8i** and evidently four ways in the case of the unsymmetrical Keim catalyst. In the case of degenerate isomerization of Ni−^{s}Bu featuring an agostic Et group (complex **8j**), the number of possible pathways is reduced by a factor of 2. In these cases, not only are the intermediate π complexes **16** and **17** expected to differ in their stability, but the barriers connecting them with the corresponding agostic alkyls must also differ.

Scheme 4. Chain-Walking Isomerization of Ni−^{n}Bu 8h to Ni−^{s}Bu 8i Complexes

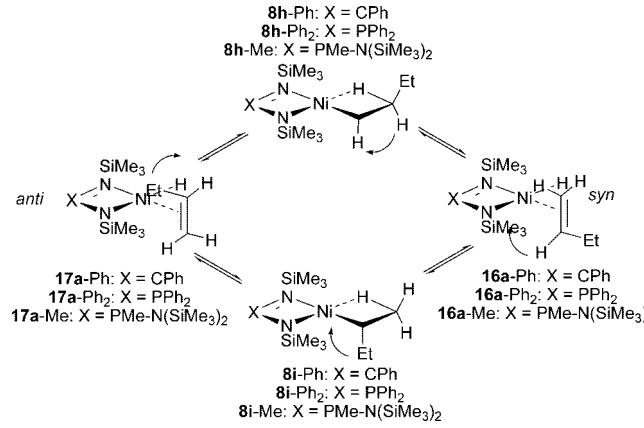

This complexity was not appreciated when this process was studied using the generic CN_2 complex, perhaps in the belief that steric effects would not be important there; certainly the isomeric, out-of-plane *syn*- and *anti*-NiH π complexes **16a** and **17a** differed little in energy in this case (vide supra). However, it can be appreciated from Scheme 4 that the isomerization pathway involving the *anti*-1-butene complex **17a**−Ph to form **8i**−Ph from **8h**−Ph involves rotation of the Et group through the space occupied by one $NSiMe_3$ group, whereas with the syn stereoisomer **16a**−Ph, it is H that undergoes a similar motion, even though the start and end points are the same. It was our expectation that the latter pathway would have a lower barrier; linear transit calculations on the unhindered Ni−PN_2 complex reinforced this view; the pathway featuring the anti stereoisomer had a 4 kcal mol^{-1} higher barrier. Therefore, in what follows, only the pathway involving the syn stereoisomer was investigated in detail.

The energies of the agostic alkyls and this intermediate along with the various TSs are summarized in Table 4. In the case of the unhindered Ni−PN_2 complex **8h**−Ph_2, the highest-energy transition structure TS **18a**−Ph_2 (ΔE = 7.8 kcal mol^{-1}) for chain walking from ^{n}Bu to ^{s}Bu is encountered in going from the agostic ^{n}Bu complex **8h**−Ph_2 to the *syn*-olefin hydride complex **16b**−Ph_2 (ΔE = 2.9 kcal mol^{-1}). A lower barrier (ΔE = 6.9 kcal mol^{-1}) connects this intermediate with the ^{s}Bu complex **8i**−Ph_2 featuring an agostic Me group. The most stable agostic alkyl is the ^{n}Bu complex, although the difference in energy is modest (1.1 kcal mol^{-1}).

Degenerate isomerization of the Ni−^{s}Bu complexes **8j**−Ph_2, featuring an agostic Et group, has a higher barrier of 9.3 kcal mol^{-1}. Here it is not possible to avoid rotating the alkene without one of the Me groups intruding into the space occupied by a $NSiMe_3$ group. We believe this steric interaction is responsible for the higher barrier seen. Very similar values were obtained for the chain-walking isomerization barriers for the corresponding Ni−CN_2 complexes **8h**−Ph and **8j**−Ph (8.1 and 11.5 kcal mol^{-1}, respectively) and the hindered Keim catalysts **8h**−Me and **8j**−Me (7.9 and 9.1 kcal mol^{-1}, respectively). In the latter case, the situation is somewhat more complicated because of the additional diastereomers possible (Scheme 5).

For example, in the case of degenerate isomerizaton of Ni−^{s}Bu complexes, there are two different agostic Et complexes, **8j**−Me and **8k**−Me. The latter is 1.1 kcal mol^{-1} lower in energy than the former. Also, the lowest-energy, intermediate π complex **16d**−Me is accessible from **8k**−Me and is 2.7 kcal mol^{-1} higher in energy than **8k**−Me. In contrast, based on linear transit calculations, only a metastable π complex **16c**−Me is

Table 4. QM Energies for Chain Walking in X(NSiMe$_3$)$_2$NiR(L) Complexes

structure	X	R	L	QM *E* (au)	ΔE (kcal mol^{-1})
8h−Ph	PhC	β-a-^{n}Bu		−4.840215	1.04
TS **18a**−Ph	PhC	β-a-^{n}Bu		−4.828967	8.1
8i−Ph$_2$	PhC	β-a-^{s}Bu	a-Me group	−4.841239	0.40
8j−Ph	PhC	β-a-^{s}Bu	a-Et group	−4.841874	0.00
TS **18c**−Ph	PhC	β-a-^{s}Bu		−4.823550	11.5
8h−Ph$_2$	Ph$_2$P	β-a-^{n}Bu		−4.840027	0.0
TS **18a**−Ph$_2$	Ph$_2$P	β-a-^{n}Bu		−4.827556	7.8
16b−Ph$_2$	Ph$_2$P	H	1-butene (*syn*-Et)	−4.835354	2.9
TS **18b**−Ph$_2$	Ph$_2$P	β-a-^{s}Bu		−4.829058	6.9
8i−Ph$_2$	Ph$_2$P	β-a-^{s}Bu	a-Me group	−4.838302	1.1
8j−Ph$_2$	Ph$_2$P	β-a-^{s}Bu	a-Et group	−4.839099	0.58
TS **18c**−Ph$_2$	Ph$_2$P	β-a-^{s}Bu		−4.825165	9.3
16c−Ph$_2$	Ph$_2$P	H	*trans*-2-butene	−4.835279	3.0
8h−Me	(Me$_3$Si)$_2$NP(Me)	β-a-^{n}Bu		−6.201635	0.24
TS **18a**−Me	(Me$_3$Si)$_2$NP(Me)	β-a-^{n}Bu		−6.189081	8.1
8i−Me	(Me$_3$Si)$_2$NP(Me)	β-a-^{s}Bu	a-Me group	−6.199286	1.7
8j−Me	(Me$_3$Si)$_2$NP(Me)	β-a-^{s}Bu	a-Et group	−6.200184	1.1
TS **18c**−Me	(Me$_3$Si)$_2$NP(Me)	β-a-^{s}Bu		−6.187459	9.1
16c−Me	(Me$_3$Si)$_2$NP(Me)	H	*trans*-2-butene	−6.193431	5.4
8k−Me	(Me$_3$Si)$_2$NP(Me)	β-a-^{s}Bu	a-Et group	−6.202023	0.0
TS **18d**−Me	(Me$_3$Si)$_2$NP(Me)	β-a-^{s}Bu		−6.178017	15.1
16d−Me	(Me$_3$Si)$_2$NP(Me)	H	*trans*-2-butene	−6.197730	2.7

Scheme 5. Chain Walking for Ni−^{s}Bu Keim Complexes 8j−Me and 8k−Me

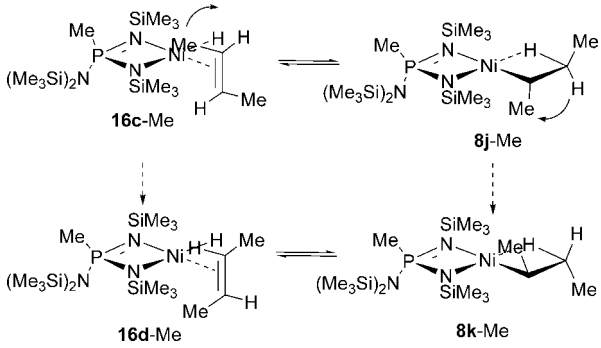

encountered during degenerate isomerization of **8j**−Me, and it is 4.2 kcal mol^{-1} higher in energy than **8j**−Me. However, the lowest barrier to rotation is actually encountered during isomerization of **8j**−Me (8.0 kcal mol^{-1} with respect to **8j**−Me) versus the situation for **8k**−Me (15.1 kcal mol^{-1}).

Complexes **8j**−Me and **8k**−Me are diastereomers and can interconvert by, e.g., β-H elimination, *trans*-2-butene dissociation, recoordination by the opposite face, and reinsertion, or if one destroys the β-agostic C−H interaction, **8j**−Me and **8k**−Me can interconvert by way of a 14-electron classical σ-alkyl complex. Either pathway involves a 14-electron intermediate at some point and is likely prohibitive from an energetic perspective. Alternatively, rotation of the PN$_2$ ligand about the Ni−P axis (or reversible dissociation of this hemilabile chelating ligand) leads to interconversion of **8j**−Me and **8k**−Me.

This latter process has a low energy barrier in the case of phosphine complexes **2a** and **2b** because only one in-plane NSiMe$_3$ signal is seen in the ^{1}H NMR spectra at room temperature ($\Delta G^{\ddagger} = 11.5 \pm 0.5$ kcal mol^{-1} for **2b** at 298 K).[11a,c] We anticipate a similar process to be facile for **8j** and related complexes, although we did not investigate it from a computational perspective (it is interesting to note, however, that during the course of this investigation higher-energy stationary points with the PN$_2$ ligand distorted toward an h^1 geometry were frequently encountered). Evidently, chain walking may occur exclusively via the less stable diasteromer **8j**−Me given the large difference in barrier heights (6.0 kcal mol^{-1}).

These results indicate that chain walking is equally facile for all three complexes. Because insertion barriers are in the order Ph$_2$P(NSiMe$_3$)$_2$NiR > PhC(NSiMe$_3$)$_2$NiR ∼ Me[(Me$_3$Si)$_2$N]P(NSiMe$_3$)$_2$NiR, one would expect branching to be most pronounced for the Ph$_2$P(NSiMe$_3$)$_2$NiR catalyst versus the Me[(Me$_3$Si)$_2$N]P(NSiMe$_3$)$_2$NiR catalyst. This is what is observed: the total branching frequency for the former complex is about 80 branches per 1000 C atoms at 298 K and 150 psig,[11c] where the latter provides a polymer with ca. 30 branches per 1000 C atoms under these conditions.[11a]

On the other hand, the predicted behavior of the PhC(NSiMe$_3$)$_2$NiR complex does not agree with what is observed upon activation of a variety of catalyst precursors with MAO (rapid formation of linear oligomers[12]), while activation of Ni−PN$_2$ complexes with MAO *also* results in the formation of linear oligomers.[11]

We suspect, based on our work with model Ni−PN$_2$ complexes and AlR$_3$,[11] that the Ni−CN$_2$ and Ni−PN$_2$ ligands are modified upon reaction with MAO or ligand abstraction is occurring. We note that complete or partial ligand abstraction would generate charged or zwitterionic nickel(II) alkyls; the activity of the species formed in situ from the nickel amidinate complexes and MAO was much more active in polar media,[12b] in agreement with this hypothesis.

4. Conclusions

The calculations reported here shed significant insight into the expected polymerization behavior of structurally related nickel amidinate and nickel iminophosphonamide complexes. The latter complexes are intrinsically more electron-rich and thus feature higher barriers to insertion; our calculations suggest that this results from a reduction in back-bonding to coordinated olefin in the transition state versus the π complex. Because bulky substituents above and below the square plane hinder chain transfer to monomer and substituents of this type are easily introduced into PN$_2$ ligands at phosphorus(V), one may have the ability to independently "tune" in-plane versus out-of-plane steric interactions in these PN$_2$ complexes. Finally, our calculations suggest that both types of complexes should be competent for forming branched polymer or oligomers from ethylene.

One thing we have not been able to account for is the incidence of long-chain (Hx$^+$) branching in PE prepared using

the Keim catalysts. Our earlier simulations easily accounted for the preponderance of Me over Et, ^{n}Pr, ^{n}Bu, etc., branching because insertion into $PN_2NiCH(Me)R$ features a significantly lower barrier compared to higher alkyls.[11a] Further, the Keim catalyst is not competent for α-olefin copolymerization, at least at room temperature, where added α-olefin acts mainly as a chain-transfer agent.[11a,b] So, macromonomer incorporation through copolymerization seems unlikely as a mechanism for LCB formation. Very recently, we observed that complex **2b** is susceptible to facile ligand C−H activation in solution at room temperature (eq 2).[22] Earlier, we had hypothesized that perhaps an intra- or intermolecular version of this process might account for LCB formation.[11a] These processes can be studied from both an experimental and a theoretical perspective and will be the subject of future work.

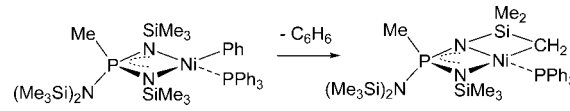

(2)

Acknowledgment. S.C. thanks The University of Akron for financial support. T.Z. acknowledges the financial support of the Natural Sciences and Engineering Research Council of Canada.

Supporting Information Available: ^{31}P NMR spectroscopic and kinetic data for the reaction of phosphorane **1** with $Ni(COD)_2$ in the presence of 1-hexene and Cartesian coordinates for all stationary points reported in this paper. This material is available free of charge via the Internet at http://pubs.acs.org.

OM700833B

(22) (a) Chai, J.; Collins, S. Unpublished observations. For related reactions involving thermolysis of L_2NiR^+ or L_2NiR_2 (R = CH_2CMe_3, etc.) complexes, see:. (b) Kitiachvili, K. D.; Mindiola, D. J.; Hillhouse, G. L. *J. Am. Chem. Soc.* **2004**, *126*, 10554–10555. (c) Miyashita, A.; Ohyoshi, M.; Shitara, H.; Nohira, H. *J. Organomet. Chem.* **1988**, *338*, 103–111.